Journal of RAMAN SPECTROSCOPY

A method for the automated Raman spectra acquisition

Journal:	*Journal of Raman Spectroscopy*
Manuscript ID	JRS-16-0297.R2
Wiley - Manuscript type:	Research Article
Date Submitted by the Author:	09-May-2017
Complete List of Authors:	Lopez-Reyes, Guillermo; Centro de Astrobiologia, Unidad Asociada UVa-CSIC Rull, Fernando; University, Fisica Materia Condesada
Keywords:	Raman, Spectroscopy, Automation, Algorithm, Optimization

SCHOLARONE™
Manuscripts

For Review

A method for the automated Raman spectra acquisition

Guillermo Lopez-Reyes (guillermo.lopez@cab.inta-csic.es), Fernando Rull Pérez.

Unidad Asociada UVa-CSIC-Centro de Astrobiología. C/ Francisco Valles 8, E-47151, Boecillo - Spain.

Key words

Raman Spectroscopy, Automation, Algorithm, Optimization

Abstract

Raman spectroscopy is a very powerful analytical technique with an increasing acceptance in the scientific community. For the optimization of the Raman acquisition, two main parameters, the integration time and the number of accumulations, need to be adjusted to the sample under analysis, as the sample, or even different spots on the same sample, can provide very different Raman responses one from another. In this paper, we present a suite of algorithms to automate the acquisition parameters adjustment to the sample under analysis, addressing issues such as spectral saturation, fluorescence, cosmic ray detection and removal, and adjustment of the acquisition parameters to optimize the acquired spectral data. This suite has been developed in the framework of the Raman Laser Spectrometer (RLS) instrument development for the Exomars mission but can be applied to any Raman spectrometer. This will allow the spectrometer to adapt to the characteristics of the sample that is being analyzed, optimizing the total operative time, while improving the usability and overall efficiency of the system.

For Peer Review

1 Introduction

1.1 Raman spectroscopy and the ExoMars mission

Raman spectroscopy is a technique for the analysis of all types of materials, minerals or biological samples, given its non-invasive and non-destructive nature. This spectroscopic technique has remained, however, unprecedented in planetary exploration, mainly due to technological limitations. However, during the last fifteen years, technology has allowed the miniaturization of Raman spectrometers to a point where they are being considered candidates for planetary missions.[1-7] The RLS instrument[8] is a 532 nm spectrometer which forms part of the payload of the rover of ESA's ExoMars mission that will be

launched to Mars in 2018. NASA Mars 2020 mission will include, onboard their future Mars rover, two different Raman devices: SHERLOC,[9] a deep-UV Raman spectrometer, and SuperCam, a combined remote Raman-LIBS-image spectrometer.[10]

In the framework of the ExoMars mission, Raman spectroscopy is a key technique, as it will provide tools for the analysis of samples from an exobiology perspective, which is the final aim of the ExoMars mission. In this direction, lots of research has been carried out in order to study the capabilities of Raman spectroscopy for the analysis of samples from an astrobiological point of view. Especially interesting is the resonant effect of carbonaceous matter, which is thus easily detected with Raman spectroscopy, and has been amply studied.[11,12] Furthermore, the interest in carbonaceous matter is not only based on the carbon-based composition of organic materials, but also supported by analysis in Martian meteorites.[13] However, there is some controversy regarding the biotic – abiotic origin of carbon based-only on the Raman spectra of the carbonaceous matter. Raman is considered necessary, but not sufficient to assess the biotic origin of this matter.[14,15] However, by complementing the Raman information with other analyses, such as optical images and structural morphology studies of the carbonaceous matter can univocally assess the biotic origin of carbonaceous matter.[16,17] In addition to carbonaceous matter *per se*, Raman spectroscopy has also been applied for the detection of biomarkers and organic materials.[18-25]

In this paper, we propose a methodology for the automated operation of a Raman spectrometer. Even if it is centered on the RLS instrument onboard the ExoMars rover, the span of applicability of the automated operation mode applied for this instrument is much wider than the exploration in the field of Earth and planetary sciences. It potentially has many medical[26-28] and industrial applications: pharmaceutical,[29,30] cosmetic,[31,32] alimentary,[32,33] or the always increasing mining industry.[34,35]. All these fields could highly profit from an automated and self-regulated Raman acquisition.

1.2 Automation of a Raman spectrometer

Given the laboratory-based nature of Raman spectroscopy on one hand, and its necessary and complex multi-parameter configuration, on the other, Raman spectroscopy has remained, to a great extent, as a technique traditionally operated with the intervention of a human operator. However, it is not possible to operate Raman spectrometers on planetary missions with such approach; the interaction with the instrument would be slow and highly inefficient (assuming it was possible). In this context, it is necessary to define means for the instrument to operate autonomously and adjust the acquisition parameters, i.e., defining the operation mode of a Raman spectrometer.

So, the operation mode of a Raman spectrometer is understood as the series of operations and algorithms that the instrument needs to perform autonomously for obtaining a Raman spectrum of the highest

For Peer Review

quality. The definition of all these algorithms is based on scientific experiments that help define objective parameters which are measurable by the instrument. This way, by monitoring those parameters, the instrument will be able to autonomously carry out those tasks that the human operator manually performs based on his experience. This experience is in general necessary to deal with the intrinsic differences found among different samples, or even different points of the same sample. These usually present strong variations in the spectrum, not only due to the existence of mixtures, but also to the different crystal orientations that can be found in powdered samples (such as the ones analyzed by the RLS instrument).

Thus, the onboard operation of the RLS instrument (and any Raman spectrometer to work autonomously) should be based on the **adaptation of the acquisition parameters to the characteristics of the sample under analysis**. This will allow saving operational time when analysing good scattering samples, which will be saved to analyse other points or samples, while maintaining a total maximum operational time. The optimization of the operation will greatly increase the science return from the instrument, while not requiring more resources.

This paper presents a suite of algorithms for the automation of the RLS instrument onboard the ExoMars rover. These algorithms allow the instrument to adjust the acquisition parameters to the sample characteristics dynamically. This will maximize the spectral quality of the acquired spectra, while also optimizing the limited resources onboard.

Even if this suite of algorithms has been created in the ExoMars mission framework, it could easily be adapted to suite any Raman spectrometer. Thus, in this paper we present a method for the automation of any software controlled Raman spectrometer, with the capability of adapting to the sample under analysis.

This paper presents the setup, samples and methodology used for the development of the algorithms, which are then generally described, detailing each of the steps in subsequent sections.

2 Setup, samples and methodology

In order to perform experiments under the operation conditions imposed by the rover, we have built and programmed the RLS ExoMars simulator.[36] This system has allowed performing the necessary scientific experiments under conditions similar to those provided by the Analytic Laboratory Drawer (ALD) of the ExoMars rover with some level of automation. Furthermore, this system has provided the means for testing the algorithms described in this work. In addition to the RLS ExoMars simulator, many data was obtained from the RLS BreadBoard system developed at INTA (Spain) as part of the RLS development,[37] in order to work with data representative of the actual RLS instrument.

For Peer Review

The basic configuration of the RLS ExoMars Simulator consists of an XYZ micrometric positioning system with an optical head attached to the Z axis, and a refillable container attached to the XY positioners. The ExoMars rover Sample Preparation and Distribution System (SPDS) carrousel and the focusing system in RLS are emulated with linear positioners (X and Z axis, respectively), assuming that the carrousel radius is big enough to be approached by a straight line. Furthermore, another axis (Y axis) was added to be able to address issues as collaborations with other instruments, in a collaborative science mode configuration.

The system implements a 532 nm continuous wave laser with a Raman optical head with a spot size of 50 microns. An internal camera allows imaging of the sample through the same optical path as the Raman probe. In addition, the Raman optical head is coupled to an external camera so that the sample can be imaged using different fields of view. With this coupled device it is possible to locate the position of the laser beam and to conduct analysis on specifically selected locations on the sample, such as making a profile of the flattened surface.

The selection of the samples used for performing the experiments is of paramount importance, as the selection can have an influence on the resulting parameterization of the automation algorithms. For our work, we used a basic set of samples (minerals and rocks), most of them considered relevant to the Mars exploration framework, and others selected for their spectral characteristics. This set includes alunite, calcite, dolomite, gypsum, silicon, quartz, clay, vermiculite, jarosite, gossan (oxide and hydroxide mineral of iron and manganese), hematite, basalt, chert and sand. In addition, other sets or samples were used to characterize the fluorescence decay, which obviously needs to be carried out with fluorescent samples. This characterization was based on spectral data from bulk and powder fluorite, fluorescent quartz and talc, as well as from mixtures of calcite and talc, and a mixture of alunite, calcite, epidote, magnesite and dolomite. All these samples have fluorescent responses when excited with the laser. In addition, several fluorescent natural samples from Tenerife island (Spain), which is considered a Martian analog,[38,39] were used for the algorithm validation.

The general methodology used for the definition of all the algorithms presented in this work is the following: study and characterization, algorithm definition, parameterization and validation/test. As already explained, the basic operational flow will be based on reference spectra that will be used to calculate and monitor key parameters by the instrument. Based on these parameters, the instrument will optimize the final acquisition process.

For Peer Review

3 Automated Raman acquisition

In order to automate a Raman spectrometer, it will be necessary to provide it with decision tools, based on which the instrument will optimize the acquisition. In our approach, the chosen operational paradigm consists on acquiring reference spectra that can be used to assess the spectral quality of the sample, and to adjust the acquisition parameters to maximize the quality of the acquired spectra, while saving operation time when the required spectral quality standards are met.

In Raman spectroscopy, there are many instrument-level parameters, especially related with the CCD device, which can be configured to optimize the acquisition and the resulting acquired spectra, such as gain, readout speed, or even its cooling temperature. Most of these parameters can be optimized for each type of sample, to improve the performance of the instrument. However, it is totally impossible to optimize all the parameters for each sample, given that the sample will not be known in advance and the Raman scattering efficiency varies several orders of magnitude from one material to another, thus, a thorough characterization of the instrument response is necessary to provide the overall best performance.

However, there are two operational-level parameters, integration time (t_i) and number of accumulations (n_a), that can be easily modified without affecting the instrument performance, but modifying the total operation time. However, several undesired effects such as fluorescence and cosmic rays can severely modify the reference spectra, and thus impair the t_i and n_a calculation performance. So, these effects need to be detected and avoided or minimized, when possible.

Taking into account these considerations, we have identified several issues that need to be addressed in order to efficiently acquire Raman spectra. This paper covers all the issues below, proposing methods for the RLS instrument to appropriately deal with them. As stated, RLS will perform the analysis based on spectra acquired as reference, taking into account the following:

- Saturation avoidance: if spectra saturate, it can lead to errors in the operation flow. Thus, it is of paramount importance that the spectra used for reference do not saturate.
- Fluorescence detection and removal: fluorescence effects are commonly found when analyzing Raman spectra (though probably not as common in Mars, due to the general lack of organics). Fluorescence can greatly reduce the SNR of the analyzed spectra. Given that fluorescence background can decrease when the sample keeps illuminated with the laser, we propose a method for automatically calculating the fluorescence quenching time based on the background decreasing rate, saving a considerable amount of time. Fluorescence and saturation avoidance are observed at the same time in the algorithm flowchart.

For Peer Review

- Cosmic ray detection and removal: we include a proposal for detecting and removing cosmic rays and spikes that can appear in the reference Raman spectra, which could cause failures in the algorithms if considered as peaks.
- Acquisition parameters adjustment: the adjustment of the integration time and the number of accumulations is performed based on the optimization of the overall operation time with a spectral-quality-based method.

Taking into account the previous considerations, the general operational flow of the automated Raman acquisition is defined (see Fig. 1). The details on each of the steps are developed in the following sections.

3.1 Saturation avoidance

As stated, the operational flow of the RLS instrument will be based on acquiring reference spectra that allow the instrument to take decisions based on the spectral characteristics of those spectra. However, it is impossible to know in advance whether the samples will be good or bad Raman scatterers, or if the sample will be fluorescent. Though we have defined a relatively short integration time for the reference spectra (t_{iref} = 1 second), it is still possible that a spectrum saturates in such a time.

In order to avoid this, our proposal is that the Raman instrument will check if the reference spectra are saturated, and, in that case, will acquire new reference spectra with a shorter integration time, with a new t_{iref} reduced by an arbitrarily set reduction factor of 40%.

3.2 Fluorescence detection and removal

An effect of particular relevance for its influence on a Raman acquired spectrum is fluorescence. This is a form of luminescence, which is the emission of light from any substance, occurring from electronically excited states. As explained by literature,[40] "in excited singlet states, the electron in the excited orbital is paired (by opposite spin) to the second electron in the ground-state orbital. Consequently, return to the ground state is spin allowed and occurs rapidly by emission of a photon". In other words, fluorescence occurs when the molecule is excited from the ground state to a discrete level of the electronic excited state. Then the excited state molecule decays to the lowest energy level via radiationless transitions. As molecules may drop down into any of several energy levels caused by deep traps on the material, the emitted photons will have different energies, and thus frequencies. This causes the appearance of radiation in different wavelengths, causing the baseline of the spectrum to grow. The lifetime of the excited state in Raman is very short (~10^{-12} to 10^{-13} s), while those in fluorescence are much longer (~10^{-7} to 10^{-9} s).[34] Thus, by using pulsed excitation sources it would be possible to reduce the fluorescence levels by time-resolving the spectral acquisition. However, most of the Raman spectrometers (including

For Peer Review

the RLS instrument) are based on a continuous wave laser excitation source, and this kind of fluorescence rejection is not possible.

It has been observed that, in fluorescence samples, if the sample keeps illuminated by the excitation source, the lower energy states tend to saturate, making the fluorescence transitions happen with lower probabilities. This is known as photobleaching, an undesired effect when performing fluorescence measurements.[40] As a result, the fluorescence emission decays and eventually stabilizes after some time. This means that the background level of consecutively acquired spectra decreases with time and then stabilizes.[41] An example for talc is shown in Fig. 2A, and for several other materials in Fig. S1 (Supporting Information). The decay and stabilization time is dependent on the sample, with times ranging from several minutes to negligible times.

3.2.1 Fluorescence decay characterization

For the development and validation of this algorithm, a selection of fluorescent samples and mixtures with different characteristics and background variation rates was used. This selection included several powdered and bulk samples of fluorite, quartz, talc and a mixture of alunite, calcite, epidote, magnesite and dolomite. In addition, several fluorescent natural samples from Tenerife (Las Cañadas, Las Arenas, Ucanca volcano…) were analysed to validate the algorithm response with a wider set of samples. For each of these samples, one second spectra were acquired with the RLS ExoMars simulator every two seconds during a total operation time of 300 seconds, providing a total number of 150 spectra of each material.

In general, the reduction of the background level of the samples implies an increase on the SNR of the spectrum, as shown in Fig. 2B, where it can be seen that there is an inverse correlation between the SNR value and the decreasing spectrum background level.[41] Thus, an algorithm for the detection and quenching of fluorescence prior to the acquisition of Raman spectra is necessary to ensure the highest possible quality of the spectra. Such an algorithm needs to deal with the problem that different materials behave differently, so setting a general fluorescence reduction time independently of the sample is highly inefficient. The algorithm should dynamically adapt to the sample under analysis.

Given the correlation existing between the SNR values and the background level of the spectrum, we have developed a procedure which is focused on comparing the variation of the background of consecutively acquired spectra until it is small enough or until an escape variable (total acquisition time or maximum number of acquired spectra) is reached. Basing the decision on the background level instead of the SNR value of the spectra highly reduces the operational complexity and resources, while increasing

For Peer Review

the robustness of the algorithm. In order to assure that the final integration time is optimally calculated, this algorithm needs to be executed at the beginning of the adjustment of the acquisition parameters.

In order to characterize the decreasing rate for different samples, we calculated the integrated spectrum area for all the spectra every 20 seconds. The background decrease rate (background level with respect to the previous spectrum) is represented for several fluorescent materials in Fig. 2C, and shows a certain convergence for all the samples. Thus, by using this parameter, it is possible to define a general algorithm, as all the samples present a similar behavior with converging values. The proposed algorithm will define a threshold for all the samples which provide a trade-off between time and background decrease, and it will illuminate the sample until the threshold value is reached, when the background level is considered to have reached an acceptable level.

It is important to note that, even if the threshold value is reached, this does not mean that the fluorescence is totally removed. Instead, it means it is reducing at lower rates than the threshold rate. If the sample was to be kept illuminated, the background would still be reduced.

3.2.2 Algorithm proposal

In order to have a functional algorithm, the total allocated time for the fluorescence quenching time needs to be limited, so there are two possible options to develop the algorithm. The first approach is to keep the sample illuminated during the total available time, while the second approach is to dynamically determine the time depending on the sample. This second option seems to be more suitable, as it will allow saving time and resources during the fluorescence reduction process that can be used for other tasks.

With this baseline, the basic operation of the algorithm consists in reducing fluorescence by comparing the relative integrated area decrement per second [%/s] of consecutive spectra. If the difference falls below a determined threshold, fluorescence is considered to have been removed to an acceptable level (though maintaining longer quenching times will, in general, further reduce the background, at smaller rates). The process also comes to an end if the total time allocated for this operation is reached. The detailed flowchart is displayed in Fig. 2D.

In general, the proposed algorithm for the quenching of fluorescence is constrained by three parameters: the maximum available time, the time elapsed between consecutive acquisitions, and the escape condition (background decrement rate). For the RLS instrument, the maximum time is 600 seconds. The elapsed time was empirically fixed to 20 seconds, and the escape condition fixed to a decreasing rate of 0.1%/s, which is a value where results showed that time had to increase highly in order to obtain small SNR improvements.

For Peer Review

3.2.3 Validation for the RLS instrument

The algorithm was evaluated with a validation set of samples from Tenerife (Spain), which were fluorescent samples in their majority. The aim was to assess the operational time that is saved by adjusting the quenching times to the sample under analysis. A total of 420 different points were analyzed, obtaining an average saved time of 147 seconds per point, in operations limited to 300 s. That is, our implementation of the fluorescence quenching algorithm managed to reduce time consumption almost 50% with respect to applying the total allocated time.

The advantages of this are straightforward: a faster acquisition, thus, a lower power consumption, which is of importance for a space mission, but also for any other Raman spectrometer.

3.3 Cosmic ray detection and removal

3.3.1 Cosmic rays and spikes in Raman spectra

Silicon detectors, including CCDs, are quite sensitive to high-energy radiation from local or extraterrestrial sources. So-called cosmic rays can in fact be cosmic rays but may also be background high-energy radiation from the lab or the CCD housing. Such events are generally infrequent but have sufficient energy to generate many electrons in the Si substrate that are stored and analyzed as if they were photoelectrons from Raman scattering. Furthermore, the incidence in Martian conditions is expected to be about 50 times higher than on Earth. The result is a large signal in one or a few pixels, which appears as a spike in the spectrum. An example of cosmic ray in a two dimensional image from a CCD can be seen in Fig. 3A. Depending on the conversion from 2D to 1D (binning to linear spectrum), and the cosmic ray incidence position, it is not uncommon to find spectral features of this kind on Raman spectra. Fig. 3B shows an example, where it can be seen how the spike that falls in the light track on the CCD in Fig. 3A is not removed by the binning process and appears in the linear spectrum.

In addition to positive spikes, CCDs often present fairly intense negative spikes that can be informally referred to as “negative” cosmic rays. These spikes should also be detected and removed by an autonomous Raman spectrometer, as they can affect following steps of the algorithms (e.g. the baseline detection).

Literature proposes several approaches for the removal of cosmic rays.[9,29,30,42,43] In summary, two different paradigms can be used for their elimination: by filtering the spikes out, or by comparing several same-condition acquired spectra. Assuming that detection based on multiple acquisitions performs better

For Peer Review

than filtering a single spectrum,[44] it was decided that a comparing paradigm for the definition of the algorithm would suit better the requirements of the instrument.

Under this baseline, we have developed a Cosmic Ray removal algorithm that compares two spectra and defines a threshold over which a point (positive or negative) is considered to be a spike. To provide a more robust performance, our proposal dynamically calculates this threshold as a function of the spectral noise. This algorithm not only allows detecting cosmic rays (positive peaks), but it also detects and removes negative spikes.

3.3.2 Algorithm proposal

The basic operation of the proposed algorithm for the detection and removal of cosmic rays consists in comparing two consecutively acquired spectra. To do so, both spectra are subtracted, and their difference is compared to a threshold related to the spectral noise, as exemplified in Fig. 3C. The detailed flowchart is displayed in Fig. 3D and F.

The algorithm uses two consecutively acquired spectra (e.g., the last spectra acquired during the fluorescence reduction process with the reference acquisition time, or the two first spectra acquired with the final integration time. It will be one or the other depending on the operation phase). These are assumed to have almost similar characteristics, except for the random spectral noise.

The difference spectrum of these spectra is calculated and, based on it, a decision threshold is defined. The following subsection will address some issues regarding the difference spectra calculation. Then, once the decision threshold is calculated, it is used to detect spectral features on the difference spectrum that are out of bounds, which would indicate the position of spikes or differences between the spectra. Then, if any spectral feature on the difference spectrum is found above the threshold (or below, for negative spikes), the values of the original spectra in those spectral positions are substituted by the interpolated values between the limits of the peak.

To avoid hard-coded parameterization of the algorithm, the threshold is defined as a value proportional to the standard deviation of the difference spectrum, i.e., proportional to the spectral noise: $a \cdot \sigma$, where "a" is a constant and σ the noise standard deviation. The values for the constant "a" can be adjusted for each instrument taking into account the spectral characteristics of the instrument. For the RLS instrument, a conservative value for "a" was 17.[41] This value was obtained by analyzing the characteristics of many spectra acquired with the RLS instrument.

For Peer Review

3.3.2.1 Difference spectrum and spectral noise value calculation

As explained, the final threshold for decision making is calculated based on the spectral characteristics of the samples under analysis, using the difference of two consecutively acquired spectra (which will have little or no differences). This is so In order to make the algorithm adaptive to the spectra under analysis, and thus independent of hard-coded parameters as much as possible,

However, experimentally for some samples, two consecutively acquired spectra can present slightly different baselines, especially when dealing with fluorescent samples (see example in Fig. 3E). This can falsely affect the noise value, leading to errors in the calculation that, in some cases, can be very important.

To deal with this issue, an intermediate step is proposed before calculating the noise standard deviation, which is to filter the spectrum to extract the "baseline" of the difference spectrum. By subtracting this "baseline" to the spectrum, the difference spectrum is always centered around zero.

A very simple and functional approach is to apply a boxcar filter (moving average) with a window size of around 13.5% of the number of points in the spectrum. For the RLS instrument (with a CCD size of 2048 pixels, this value was fixed to 151). This configuration of the filter is enough to remove most of the high-frequency variation of the difference spectrum, providing a good "baseline" of the difference spectrum. By removing this curve, the difference spectrum is unbiased, providing much more accurate results. This approach is therefore always included as a baseline for the noise calculation routine, as per the flowchart in Fig. 3D and F. An example showing how this subroutine works is displayed in Fig. 3E.

3.3.3 Validation for the RLS instrument

Though originally this algorithm was intended for the detection of cosmic rays that saturated the CCD (or that are many times higher than the spectral peaks), we applied the algorithm with the configuration described above to the spectra from our RLS test database that presented non-saturating spikes, to test the detection range of the algorithm. An example of the algorithm correctly detecting and removing relatively small spikes can be seen in Fig. 3C. The results show that the most potentially dangerous spikes are removed with this algorithm and the nominal threshold values (20% margin).

However, in some cases, the algorithm fails to properly remove some of the spikes. Fortunately, in all cases, the spikes that escaped the threshold were below the signal value. In any case, it might be interesting to include a final filtering stage (a moving average of a very small window, 3 pixels, for example) to reduce the amplitude of the spikes without really affecting the spectrum. Large windows might affect the behavior of the final t_i calculation algorithm, so it is important to keep this filter size small. The use of this post-processing stage would minimize greatly the risk of errors due to those

For Peer Review

undetected spikes, while not representatively impacting the following stages of operation. Even though for RLS we decided to use this kind of filter, any other type of filter might work, as long as it does not filter the most relevant spectral features (peaks) of the spectra.

3.4 Adjustment of the acquisition parameters

The Raman scattering efficiency of the materials that a typical Raman spectrometer will analyze can present differences of several orders of magnitude. Unhappily, the dynamic range of the spectrometers cannot be used to compensate this scattering range without adjusting the acquisition parameters. There are two key operational-level parameters that can be adjusted when performing Raman spectroscopy: the integration time (t_i) and the Number of Accumulations (n_a).

Following, a study of the spectral quality of the acquired spectra as a function of these two parameters is presented. This study is used to develop and propose an algorithm for the automated calculation of these parameters, based on the spectral response of the sample under analysis. With this algorithm it will be possible to optimize the acquired spectral quality, while reducing the total operation time. To do so, the SNR of the spectrum is characterized as a function of n_a, in such a way that it will be possible to progressively reduce n_a with higher SNR values.

3.4.1 Spectral SNR characterization as a function of t_i & n_a

3.4.1.1 SNR maximization as function of (t_i, n_a)

The Raman acquisition process can be adjusted by modifying the integration time, t_i, and the number of accumulations, n_a .These two parameters directly affect the total operation time, which is calculated as n_a * t_i. In order to evaluate the spectral quality based on these parameters, several five-minute spectra were acquired with different (t_i, n_a) combinations, for three different materials with different scattering efficiencies (calcite, silicon and gossan). For the three materials, the SNR of each spectrum was calculated. To make the curves comparable in the same graph for all the samples (i.e., to compensate the materials different efficiency), they were normalized and centered by subtracting their average and dividing them by their standard deviation (this graph is represented in Fig. 4A). The results show that, for spectra acquired with equivalent total operation times (300 seconds), the SNR is higher for higher integration times than for higher numbers of accumulations. One of the reasons is that for higher integration times, the CCD needs to be read fewer times, highly reducing the contribution of the readout noise to the spectrum SNR. The implication of this result is quite straightforward: any automation algorithm will need to **optimize** t_i **first, and then** n_a, assuming a finite total operation time.

For Peer Review

3.4.1.2 t_i Characterization

It is well known that, in Raman spectroscopy, the higher the integration time, the higher the acquired signal intensity and SNR. Furthermore, Raman emission is a scattering process which happens with higher probability as a function of the excitation source flux of photons. Given that a CW laser provides a constant flux of photons, it is expected that the number of Raman photons emitted by the sample and received by the CCD will be constant per time unit.

The CCD response to light is quite linear when the saturation level is in the dynamic range of the CCD, as the dark current levels are usually negligible (in the case of RLS, <10 electrons per pixel per second for an inverted mode CCD). This is so, even experimentally, at the working temperature of the CCD installed in the RLS breadboard system used during the spectra acquisition (this might be different if the CCD was a non-inverted mode one).

On the other hand, the bias level of the CCD can influence the calculations if not taken into account, especially for poor Raman scatterers. Thus, the **intensity increase is constant with time** when taking into account the effect of the bias level. Fig. 4B presents the intensity at one pixel with respect to the integration time. It can be seen that the linear adjustment provides an R-square value of 1. Of course, this does not imply that the SNR also increases linearly.

However, given that the integration time needs to be calculated first for the automatic adjustment of the parameters, as justified above, it is the intensity that will be parameterized with the algorithm, instead of the SNR of the resulting spectra, relieving the processor from the extra computational load that would be necessary to perform these calculations. The criterion chosen to define the integration time is to have the spectral intensity cover 80% of the dynamic range of the CCD.

3.4.1.3 n_a characterization

As it is also well known, the accumulation of several consecutively acquired spectra reduces the noise of the averaged spectrum. However, as shown above, the SNR increase associated with higher numbers of accumulations is lower than the SNR increase provided by higher integration times. Nevertheless, once t_i has been calculated to cover 80% of the dynamic range of the CCD, the rest of the available operational time can be used to acquire and average several spectra to increment the SNR.

In order to characterize the SNR increase with respect to the number of accumulations, several spectra of silicon, calcite and gossan with several integration times were acquired and analysed. By accumulating those spectra with different numbers of accumulations, and calculating their SNR, the SNR evolution with respect to n_a was obtained for different materials and integration times. Fig. 4C shows the curves, normalized for representation purposes. As it can be seen, only up to 150 accumulations are represented

For Peer Review

for the t_i = 1s spectra, while only 50 for the t_i = 3s spectra, and so on. This is due to the fact that the total operation time during the test was set for these samples to 300 seconds, and the fact that, to calculate the SNR of a spectrum it is necessary to subtract two of them consecutively. Thus, it is only possible to have 50 accumulations of spectra with t_i = 3s, 30 spectra for t_i = 5s, 10 spectra for t_i = 10s, and so on.

This representation shows that the **SNR evolution is similar for different spectra,** not only when acquired with the same integration time, but also with different t_i's. Actually, the correlation value between the curves is higher than 95%.

Given the similarity in the curves for spectra with different integration times, we used the average SNR evolution for the t_i = 1 s spectra to fit the SNR evolution to a power function. Fig. 4D represents this curve, normalized to the SNR of a single (non-accumulated) spectrum. Thus, this figure represents the factor by which the SNR gets multiplied when accumulating different numbers of spectra, or alternatively, the SNR increment in parts per unit. It is interesting to see how the SNR evolution is proportional to the square root of n_a with an R-square value very close to 1.

3.4.2 Algorithm proposal

The optimal way to adjust the acquisition parameters is to calculate the final integration time first, and then the number of accumulations, as a function of the available time. In addition, the proposed algorithm progressively reduces the value of NA with increasing values of SNR (the higher SNR, the lower the necessary n_a). This is done in order to save operational time when a minimum spectral quality is achieved.

3.4.2.1 Integration time calculation

In order to calculate the integration time, it is important to make sure that no pixel of the CCD saturates. However, in order to avoid operational load, the calculation of the pixel of the CCD ROI (Region of interest) that contains the spectrum maximum intensity will be decided based on the binned (1D) spectrum that was used for the previous stages (fluorescence and cosmic ray detection). By using the maximum position of this spectrum it is possible to locate the maximum intensity among all the pixels in the corresponding column in the ROI. However, it is necessary to take into account the list of cosmic rays removed from the 1D spectrum, as these will not be removed from the 2D spectrum. To solve this issue, in case the maximum position coincides with a cosmic ray, the next maximum of the spectrum will be used as the maximum intensity point.

The maximum intensity is the intensity obtained for the reference spectrum integration time ($t_{i\text{-}ref}$ = 1 second). In addition, in order to ensure the linearity of the signal increase with time, it is necessary to subtract the bias level of the CCD, as shown in the following equation.

For Peer Review

$$t_{i-final} = \frac{0.8 \cdot CCD\_dynamic\_range}{maximum - bias - darkCurrent \cdot t_{i-ref}} \cdot t_{i-ref}$$

The only other limitation for the RLS instrument is, assuming a total acquisition time of 5 to 10 minutes, is the maximum integration time of **Final $t_i \leq 60$ s**. The reason to choose this value is that it is necessary to acquire dark spectra of the same integration time. The longer t_i, the higher the time spent without acquiring "relevant" Raman signal. Fig. 5A shows the detailed flowchart for the calculation of the final integration time.

3.4.2.2 Calculation of the Number of Accumulations

The calculation of the number of accumulations is based on the spectral quality of two reference spectra acquired with the final t_i. The reason to have two of them is to reject the possible cosmic rays or spikes that can appear in the spectra, and that can hamper the automatic calculation of the SNR. The calculated SNR value will be used to determine the spectral quality and the necessary n_a to increment the SNR as in Fig. 4D, to reach the minimum quality standards required by each specific application. Other parameters that have to be adjusted to their corresponding application are the limits imposed by the operational constraints, such as minimum and maximum number of accumulations, or maximum total operation time (t_i*n_a), which cannot be exceeded. In addition, limits for SNR and NA need to be established. For values below a determined SNR, the maximum possible n_a will be acquired. For values over the desired SNR value, the minimum one will be acquired.

To define the minimum acceptable value of SNR, we performed a study on the baseline correction errors by evaluating all the "false peaks" detected by the algorithm, and calculating their SNR. With this calculation, for the RLS instrument, the minimum SNR value was set to $\mathbf{SNR_{min} = 30}$. The SNR value that would be desirable for all the samples (target SNR, or SNR_{max}) is set to $\mathbf{SNR_{max} = 120}$, which is twice the SNR obtained with RLS with a 10 minutes spectrum of gossan (t_i =60s, n_a=10), considered one of the worst scatterers that is expected to be found on Mars.

Finally, the n_a limits were set between 4 and 150 to ensure that at least some accumulations are performed in each case, while providing margin enough to get to high numbers of accumulations: $\mathbf{n_{a\ min} = 4}$ **and** $\mathbf{n_{a\ max} = 150}$.

Taking all these issues into consideration, the final calculated value of n_a will be defined by the following logic, which calculates values of n_a both based on quality as well as on the available time. The most restrictive is finally selected.

Based on SNR:

For Peer Review

if SNR<SNR_{min} -> $n_{a\ aux} = n_{a\ max}$

else if SNR >SNR_{max} -> $n_{a\ aux} = n_{a\ min}$

else calculate $n_{a\ aux}$ to get SNR_{max} (from Figure 18)

Based on available time:

If $(n_{a\ aux} + 1) * \text{final } t_i < \text{max\_operation\_time}$ then final $n_a = n_{a\ aux}$

else final n_a = floor (max_operation_time / final t_i) - 1

The general flowchart to calculate the number of accumulations is described in Fig. 5B. It is important to note that the SNR value for this algorithm needs to be calculated as part of the algorithm. This paper does not include the description of this calculation due to editorial constraints, but the proposal for the automated calculation of the SNR for the RLS instrument can be found in the PhD Thesis by G. Lopez-Reyes.[41]

3.4.2.3 Validation for the RLS instrument

The intent of dynamically adjusting the acquisition parameters is to save operation time when the spectral quality is above a determined threshold. For the development and validation of this algorithm, we used a spectral database including the following samples: silicon, calcite, vermiculite, gypsum, alunite, basalt, dolomite, hematite (two different types), clay, jarosite, chert, a mixture of clay and sand, quartz and gossan. All these samples were analyzed with the parameters calculated by the algorithm, and the SNRs of the final spectra were calculated.

The results showed that acquisition time is saved by adjusting the parameters. In average, the algorithm saved 334 seconds per sample, while ensuring SNR values equal or higher to the expected ones (with an average SNR surplus of 20), and which is in most cases higher than the desired SNR value (120).

Fig. S2 (Supporting Information) depicts the correlation between the expected and the final SNR for the samples. As it can be seen, the correlation is quite linear, with a slope higher than 1, which implies that the calculated final SNR is in general higher than the expected one (explaining the average SNR surplus explained above). The fact that the final SNR is higher than the expected ensures the robustness of the algorithm, which guarantees a minimum level of quality, as long as there are time resources available.

The proposed algorithm for the automated calculation of the acquisition parameters onboard the RLS has shown an important potential reduction of the operation time, without compromising the quality standards of the acquired spectra. At RLS level, the remainder of the time could be used to acquire more samples at

For Peer Review

different spots. From the scientific point of view, this possibility is key to obtain the best science return from the instrument, and not performing in such a way would imply a very important loss of capabilities and science scope.

4 Summary and conclusions

We have presented a suite of algorithmic procedures to procure an automated and optimized Raman acquisition. This suite includes algorithms for the proper management of spectral saturation, fluorescence and cosmic ray detection and removal, and for the automatic calculation of the optimal acquisition parameters, which will be done based on the quality of spectra of reference.

The fluorescence reduction algorithm is one of the most important algorithms to apply in order to save operational time, as it will allow reducing the quenching time as a function of the sample response (based on the background decreasing rate per second). This is very important as the allocated time for fluorescence is relatively high, while not all samples to be analyzed will be fluorescent. Thus, the implemented approach has been designed in order to not have a considerable impact on the operation time for non-fluorescent samples. The algorithm limits the time consumption for quenching when the samples are not fluorescent.

The basic operation of the acquisition parameters adjustment is based on the calculation of spectral parameters from reference spectra acquired prior to the final acquisition. These parameters (e.g. the spectral quality) will be used by the algorithms to take decisions on the final acquisition parameters. Thus, spurious peaks or spikes such as cosmic rays might be critical for the correct functioning of the algorithms. In order to minimize the effect of this kind of effects, a dedicated algorithm was implemented for the detection and removal of spikes. This algorithm was based on comparing two spectra and detecting all differential spectral features between them. As a result, many of the spurious detected during our tests were corrected, improving the end-to-end behavior of the system.

Finally, the adjustment of the integration time and number of accumulations is based on adjusting t_i to fill 80% of the dynamic range of the CCD, while the number of accumulations is decided based on the spectral characteristics of the reference spectra (the higher the SNR, the lower the necessary number of accumulations).

The definition of any algorithm needs to follow the same development structure: problem description and characterization, algorithm proposal, parameterization (optimization) and validation. For this work, each

For Peer Review

algorithm was defined, implemented, parameterized, optimized and validated with the RLS ExoMars Simulator, in order to be implemented onboard the RLS instrument.

Even if this suite of algorithms has been proposed in the framework of the development of the RLS instrument, it could in principle be applied for any Raman system that needs to adjust the acquisition to the sample under analysis, and to optimize the operational resources and time of any Raman spectrometer. The application of this work can definitely help improve the usability of Raman spectroscopy both in laboratory and portable spectrometers, multiplying its effectiveness without impairing the quality of the acquired spectra.

5 References

[1] A. Ellery, D. Wynn-Williams, *Astrobiology.* **2003**; *3*, 565.
[2] A. Wang, L. A. Haskin, A. L. Lane, T. J. Wdowiak, S. W. Squyres, R. J. Wilson, L. E. Hovland, K. S. Manatt, N. Raouf, C. D. Smith, *J. Geophys. Res.* **2003**; *108*, 5005.
[3] S. K. Sharma, P. G. Lucey, M. Ghosh, H. W. Hubble, K. A. Horton, *Spectrochimica Acta Part A: Molecular and Biomolecular Spectroscopy.* **2003**; *59*, 2391.
[4] S. M. Angel, N. R. Gomer, S. K. Sharma, C. McKay, *Applied Spectroscopy.* **2012**; *66*, 137.
[5] R. C. Wiens, S. K. Sharma, S. M. Clegg, A. K. Misra, P. G. Lucey In *Seventh International Conference on Mars*; Lunar and Planetary Institute: Houston, 2007, p Abstract #3092.
[6] D. L. Dickensheets, D. D. Wynn-Williams, H. G. M. Edwards, C. Schoen, C. Crowder, E. M. Newton, *Journal of Raman Spectroscopy.* **2000**; *31*, 633.
[7] A. Ellery, D. Wynn-Williams, J. Parnell, H. G. M. Edwards, D. Dickensheets, *Journal of Raman Spectroscopy.* **2004**; *35*, 441.
[8] F. Rull, S. Maurice, E. Diaz, C. Tato, A. Pacros, t. R. Team. In *42nd Lunar and Planetary Science Conference LPSC*; Lunar and Planetary Institute: Houston, 2011, p Abstract #2400.
[9] L. Beegle, R. Bhartia, L. DeFlores, M. Darrach, R. Kidd, W. Abbey, S. Asher, A. Burton, S. Clegg, P. Conrad, *LPI Contributions.* **2014**; *1783*, 5101.
[10] O. Gasnault, S. Maurice, R. Wiens, S. Le Mouélic, W. Fischer, P. Caïs, K. McCabe, J.-M. Reess, C. Virmontois In *Lunar and Planetary Science Conference* 2015; Vol. 46, p 2990.
[11] E. Quirico, G. Montagnac, J.-N. Rouzaud, L. Bonal, M. Bourot-Denise, S. Duber, B. Reynard, *Earth and Planetary Science Letters.* **2009**; *287*, 185.
[12] A. C. Ferrari, *Solid State Communications.* **2007**; *143*, 47.
[13] A. Steele, F. McCubbin, M. Fries, L. Kater, N. Boctor, M. Fogel, P. Conrad, M. Glamoclija, M. Spencer, A. Morrow, *Science.* **2012**; *337*, 212.
[14] J. D. Pasteris, B. Wopenka, *Astrobiology.* **2003**; *3*, 727.
[15] C. P. Marshall, H. G. Edwards, J. Jehlicka, *Astrobiology.* **2010**; *10*, 229.
[16] J. W. Schopf, A. B. Kudryavtsev, D. G. Agresti, T. J. Wdowiak, A. D. Czaja, *Nature.* **2002**; *416*, 73.
[17] J. W. Schopf, A. B. Kudryavtsev, D. G. Agresti, A. D. Czaja, T. J. Wdowiak, *Astrobiology.* **2005**; *5*, 333.
[18] A. Culka, J. Jehlička, P. Vandenabeele, H. Edwards, *Spectrochimica Acta Part A: Molecular and Biomolecular Spectroscopy.* **2011**; *80*, 8.
[19] A. Culka, J. Jehlička, L. Strnad, *Spectrochimica Acta Part A: Molecular and Biomolecular Spectroscopy.* **2012**; *86*, 347.
[20] H. G. Edwards, *Origins of Life and Evolution of the Biosphere.* **2004**; *34*, 3.

For Peer Review

[21] H. G. Edwards, I. B. Hutchinson, R. Ingley, J. Parnell, P. Vítek, J. Jehlička, *Astrobiology.* **2013**; *13*, 543.
[22] J. Jehlička, H. Edwards, P. Vítek, *Planetary and space Science.* **2009**; *57*, 606.
[23] P. Vandenabeele, J. Jehlička, P. Vitek, H. Edwards, *Planetary and Space Science.* **2012**; *62*, 48.
[24] P. Vítek, J. Jehlička, H. G. Edwards, I. Hutchinson, C. Ascaso, J. Wierzchos, *Astrobiology.* **2012**; *12*, 1095.
[25] P. Vítek, K. Osterrothová, J. Jehlička, *Planetary and Space Science.* **2009**; *57*, 454.
[26] R. Mateus, H. Abdalghafor, G. Oliveira, J. Hadgraft, M. E. Lane, *International Journal of Pharmaceutics.* **2013**; *444*, 106.
[27] P. Matousek, N. Stone, *Journal of biophotonics.* **2013**; *6*, 7.
[28] I. Barman, N. C. Dingari, A. Saha, S. McGee, L. H. Galindo, W. Liu, D. Plecha, N. Klein, R. R. Dasari, M. Fitzmaurice, *Cancer Research.* **2013**; *73*, 3206.
[29] G. Févotte, *Chemical Engineering Research and Design.* **2007**; *85*, 906.
[30] T. De Beer, A. Burggraeve, M. Fonteyne, L. Saerens, J. P. Remon, C. Vervaet, *International Journal of Pharmaceutics.* **2011**; *417*, 32.
[31] D. Kurouski, R. P. Van Duyne, *Analytical Chemistry.* **2015**; *87*, 2901.
[32] L. Pereira, S. F. Gheda, P. J. Ribeiro-Claro, *International Journal of Carbohydrate Chemistry.* **2013**; *2013*, 7.
[33] I. Delfino, C. Camerlingo, M. Portaccio, B. D. Ventura, L. Mita, D. G. Mita, M. Lepore, *Food Chemistry.* **2011**; *127*, 735.
[34] T. Kauppinen, N. Khajehzadeh, O. Haavisto, *International Journal of Mineral Processing.* **2014**; *132*, 26.
[35] M. De Biasio, T. Arnold, G. McGunnigle, R. Leitner, A. Tortschanoff, N. Fietz, L. Weitkämper, D. Balthasar, V. Rehrmann, In *Proc. SPIE*, 2012; Vol. 8374, p 83740S.
[36] G. Lopez-Reyes, F. Rull, G. Venegas, F. Westall, F. Foucher, N. Bost, A. Sanz, A. Catalá-Espí, A. Vegas, I. Hermosilla, A. Sansano, J. Medina, *European Journal of Mineralogy.* **2013**; *25*, 721.
[37] E. Díaz, A. G. Moral, C. P. Canora, G. Ramos, O. Barcos, J. A. R. Prieto, I. B. Hutchinson, R. Ingley, M. Colombo, R. Canchal, B. Dávila, J. A. R. Manfredi, A. Jiménez, P. Gallego, J. Pla, R. Margoillés, F. Rull, A. Sansano, G. López, A. Catalá, C. Tato, In *Proc. SPIE*, 2011; Vol. 8152, p 81520L.
[38] E. Lalla, G. Lopez-Reyes, F. Rull, J. Martinez-Frías, A. Sansano, R. Navarro, J. Medina In *44th Lunar and Planetary Science Conference*; Lunar and Planetary Institute: Houston, 2013, p Abstract #2403.
[39] E. A. Lalla, G. López-Reyes, A. Sansano, A. Sanz-Arranz, D. Schmanke, G. Klingelhöfer, J. Medina-García, J. Martínez-Frías, F. Rull-Pérez, *Estudios geologicos.* **2015**; *71*, e035.
[40] J. Lakowicz *Principles of Fluorescence Spectroscopy*; Kluwer Academic/Plenum Publishers, **1999**.
[41] G. Lopez-Reyes *Development of algorithms and methodological analyses for the definition of the operation mode of the Raman Laser Spectrometer instrument*, Universidad de Valladolid, **2015**.
[42] A. Sansano, R. Navarro, J. Medina, J. Manrique-Martinez, G. Lopez-Reyes, F. Rull, *LPI Contributions.* **2014**; *1783*, 5096.
[43] Y. Katsumoto, Y. Ozaki, *Applied spectroscopy.* **2003**; *57*, 317.
[44] R. L. McCreery *Raman Spectroscopy for Chemical Analysis*; John Wiley & Sons, Inc., **2000**.

For Peer Review

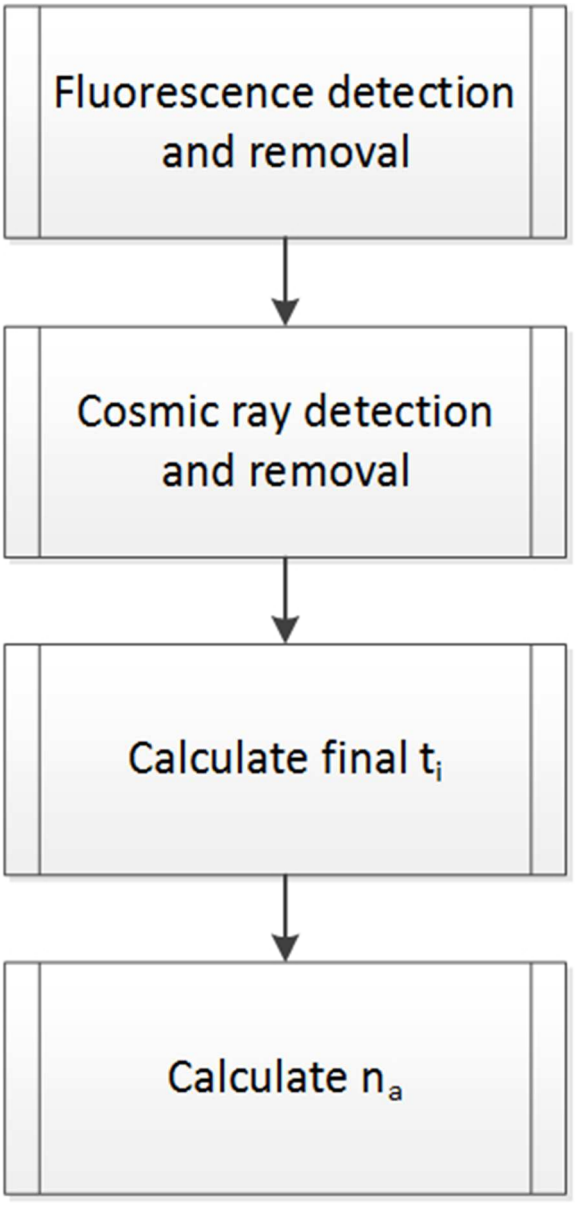

Figure 1. General operation flowchart

49x103mm (150 x 150 DPI)

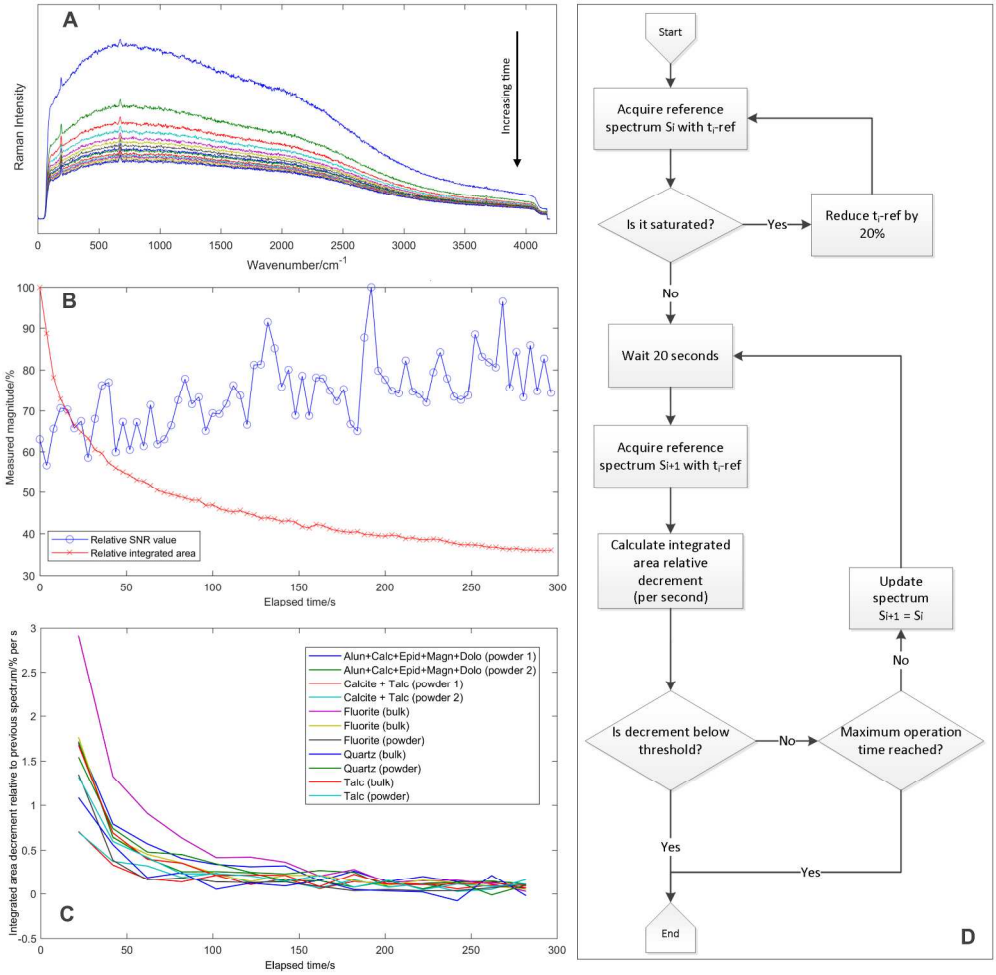

Figure 2. Fluorescence decay evolution for talc (A): spectrum background decreases with time. SNR and fluorescence background level evolution of talc with excitation time (B). Spectral relative area decrement for different materials (C). Flowchart of the fluorescence reduction algorithm (D).

798x776mm (96 x 96 DPI)

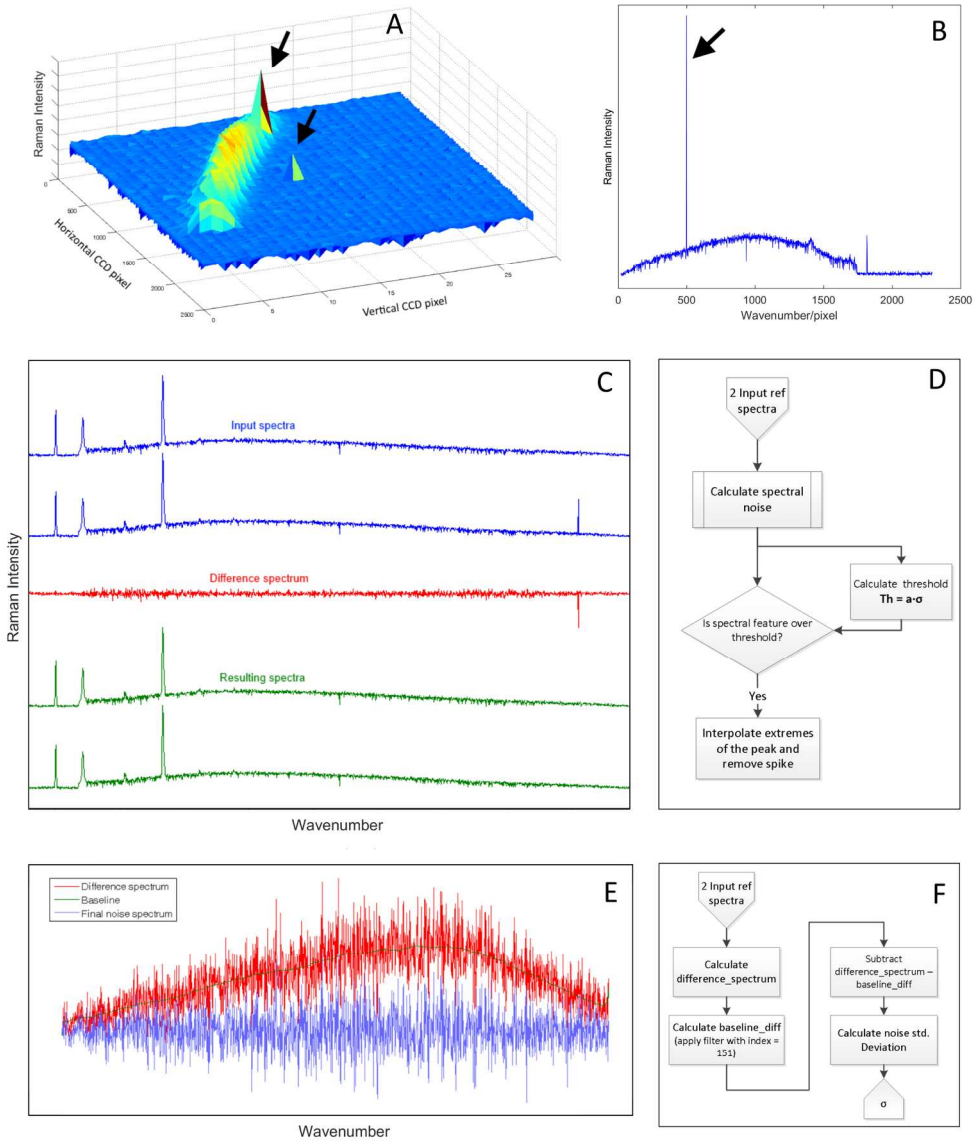

Figure 3. Cosmic ray examples in two dimensional (A) and binned (B) spectra. Example of cosmic ray/spike removal (C). Flowchart of the cosmic ray/spike detection algorithm (D). Offset removal from difference spectrum (E). Flowchart of the "Calculate spectral noise" block in D (F).

547x646mm (96 x 96 DPI)

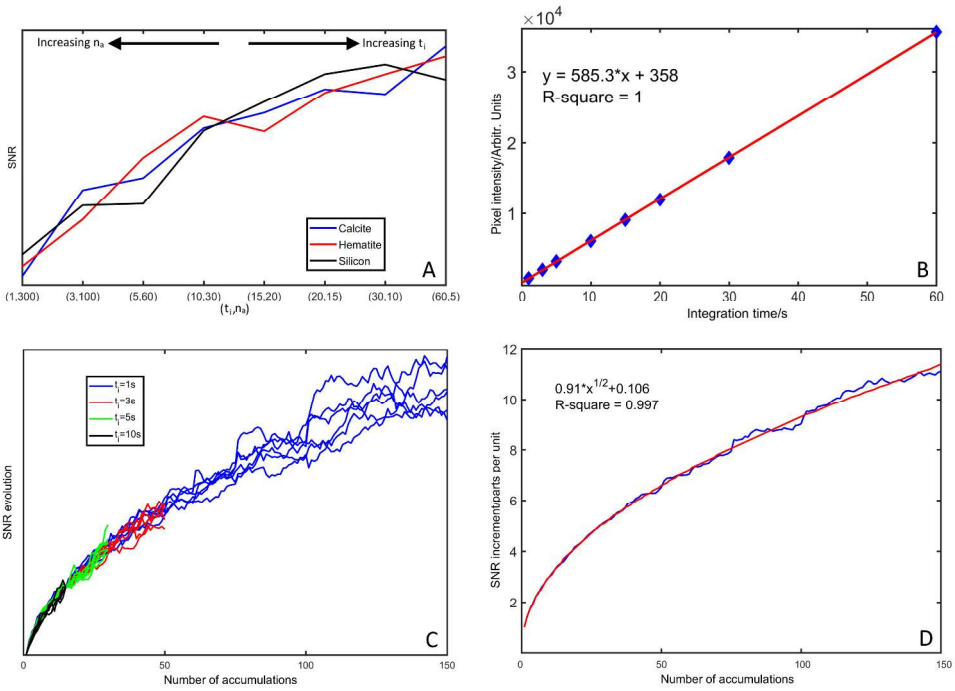

Figure 4. SNR evolution for different combinations of acquisition parameters. All spectra were acquired during a total operation time of 300 seconds. Data is normalized and centered for visualization (A). Intensity at one CCD pixel vs. Integration time (B). SNR evolution for different numbers of accumulations, for different integration times and samples (C). SNR multiplying factor for different numbers of accumulations (D)

1058x749mm (96 x 96 DPI)

view

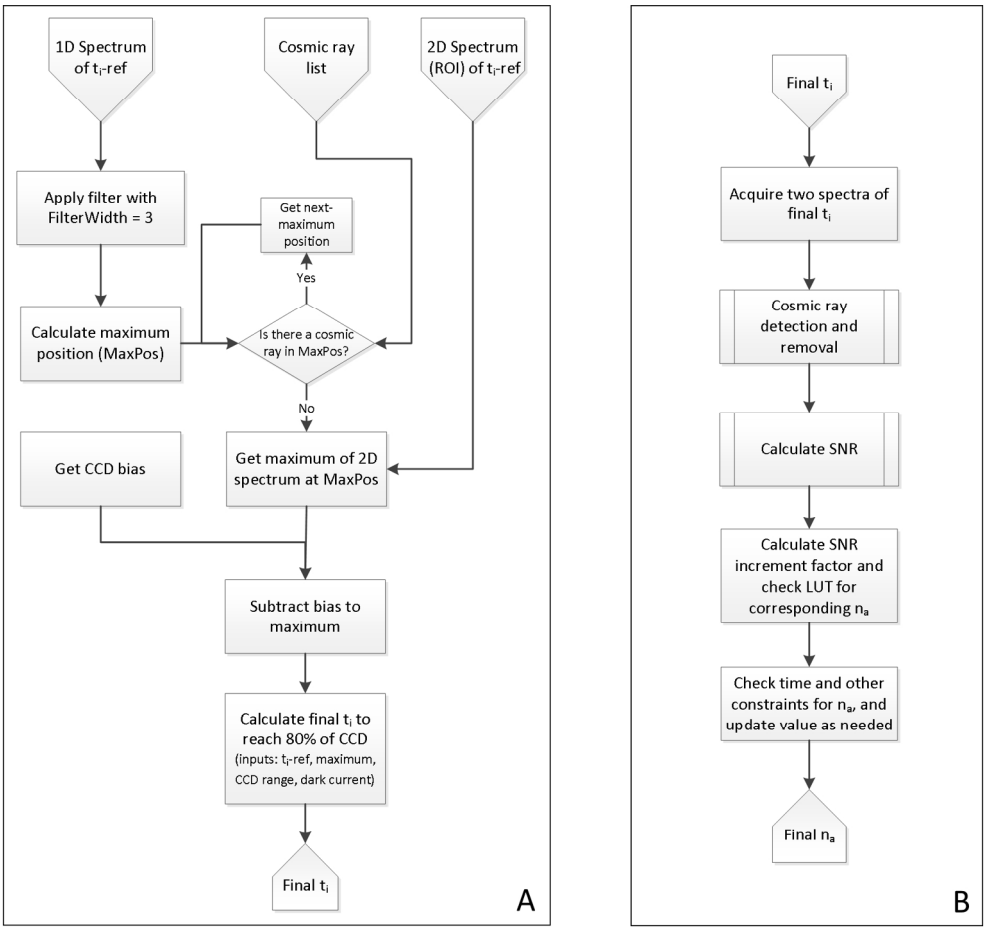

Figure 5. Flowchart for the calculation of the final integration time (A) and the number of accumulations (B).

507x476mm (96 x 96 DPI)

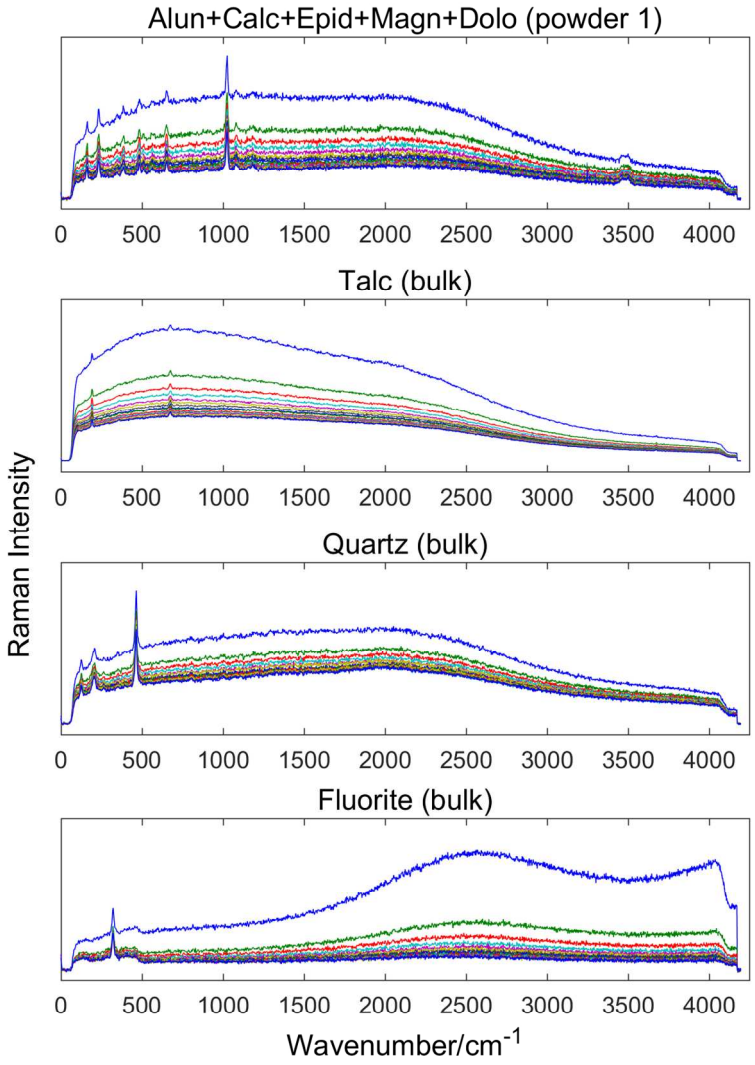

Figure S1. Fluorescence background decay evolution with time for different materials. As time passes, the spectra background reduces.

385x521mm (96 x 96 DPI)

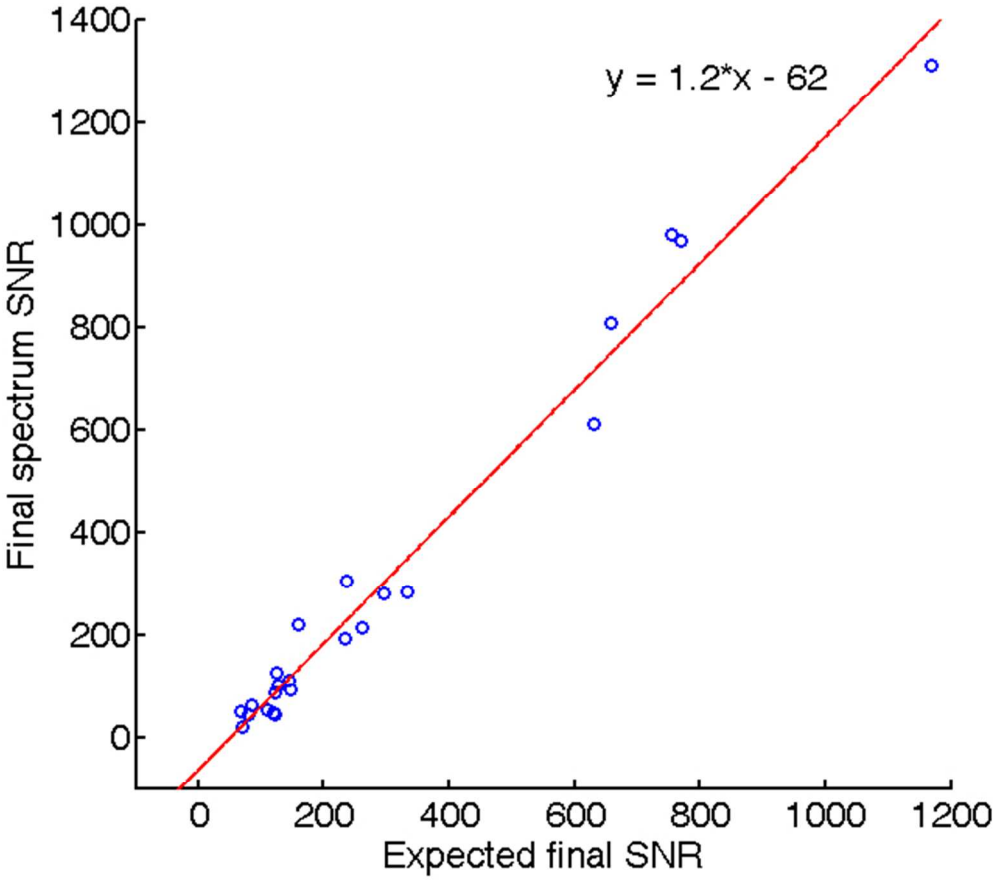

Figure S2. Correlation between theoretical and experimental SNR

170x150mm (96 x 96 DPI)